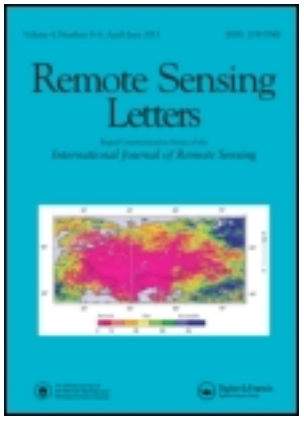

Remote Sensing Letters
Publication details, including instructions for authors and subscription information:
http://www.tandfonline.com/loi/trsl20

Assessing water quality in the northern Adriatic Sea from HICO™ data

Federica Braga [a], Claudia Giardino [b], Cristiana Bassani [c], Erica Matta [b], Gabriele Candiani [b], Niklas Strömbeck [d], Maria Adamo [e] & Mariano Bresciani [b]

[a] Institute of Marine Sciences (ISMAR-CNR), 30122, Venezia, Italy

[b] Institute for Electromagnetic Sensing of the Environment (IREA-CNR), 20133, Milano, Italy

[c] Institute of Atmospheric Pollution Research (IIA-CNR), 00016, Monterotondo Scalo, Roma, Italy

[d] Strömbeck Consulting, SE-121 52, Johanneshov, Sweden

[e] Institute of Intelligent Systems for Automation (ISSIA-CNR), 70126, Bari, Italy

To cite this article: Federica Braga, Claudia Giardino, Cristiana Bassani, Erica Matta, Gabriele Candiani, Niklas Strmbeck, Maria Adamo & Mariano Bresciani (2013) Assessing water quality in the northern Adriatic Sea from HICO™ data, Remote Sensing Letters, 4:10, 1028-1037, DOI: 10.1080/2150704X.2013.830203

To link to this article: http://dx.doi.org/10.1080/2150704X.2013.830203

Remote Sensing Letters, 2013
Vol. 4, No. 10, 1028–1037, http://dx.doi.org/10.1080/2150704X.2013.830203

Assessing water quality in the northern Adriatic Sea from HICO™ data

FEDERICA BRAGA*†, CLAUDIA GIARDINO‡, CRISTIANA BASSANI§, ERICA MATTA‡, GABRIELE CANDIANI‡, NIKLAS STRÖMBECK¶, MARIA ADAMO| and MARIANO BRESCIANI‡

†Institute of Marine Sciences (ISMAR-CNR), 30122 Venezia, Italy
‡Institute for Electromagnetic Sensing of the Environment (IREA-CNR), 20133 Milano, Italy
§Institute of Atmospheric Pollution Research (IIA-CNR), 00016 Monterotondo Scalo, Roma, Italy
¶Strömbeck Consulting, SE-121 52 Johanneshov, Sweden
|Institute of Intelligent Systems for Automation (ISSIA-CNR), 70126 Bari, Italy

(*Received 3 June 2013; accepted 26 July 2013*)

This letter focuses on water-quality estimation in the northern Adriatic Sea using physically-based methods applied to image obtained with the Hyperspectral Imager for the Coastal Ocean (HICO™). Optical properties of atmosphere and water were synchronously measured to parameterise such methods. HICO™-derived maps of chlorophyll-*a* (chl-*a*) and suspended particulate matter (SPM) indicated low values, in the range of 0–3 mg m^{-3} and 0–4 g m^{-3}, respectively, correlating significantly with field data ($R^2 = 0.71$ for chl-*a* and $R^2 = 0.85$ for SPM). The results, on analysis, identify clear waters in the open sea and moderately turbid waters near the coast due to river sediment discharge and organic matter from coastal lagoons. These findings support the use of HICO™ data to assess water-quality parameters in coastal zones and suggest the feasibility of integrating them with future-generation space-borne hyperspectral images.

1. Introduction

Coastal zones are important interfaces between land, sea and atmosphere, acting as a boundary for oceanic circulation and currents, as well as receiving inputs from the land. River discharge, wind energy, tidal mixing and long-shore currents influence the distribution of suspended and dissolved matter in coastal zones, varying their concentration, size and physical–chemical composition. The organic component, be it dissolved or particulate, is also generated and converted within the coastal system (by photosynthesis and degradation) and its distribution may vary considerably. The impact of human activities (e.g. changes in land use, sewage discharge, aquaculture industry and port activities) on coastal ecosystems further increases their variability.

The Hyperspectral Imager for the Coastal Ocean (HICO™) is the first space-borne hyperspectral sensor designed specifically for the coastal ocean and for estuarine,

*Corresponding author. Email: federica.braga@ismar.cnr.it

riverine, lacustrine and other shallow-water areas. The HICO^{TM} acquires images from different angles in selected areas, at various times of day. Each pixel covers 90 × 90 m, with 87 nominal spectral channels in the range of 400–900 nm providing information on water properties and bottom reflectance (see Lucke *et al.* 2011).

HICO^{TM} images have been proved to be useful for estimating chlorophyll-*a* (chl-*a*) (Gitelson *et al.* 2011), as well as for monitoring suspended sediments in river plumes (Tufillaro *et al.* 2010). Most of the related studies focused on very turbid and productive waters, applying semi-empirical algorithms optimized for HICO^{TM} spectral bands. In the present study, the aim is instead to use the HICO^{TM} data for assessing water quality in moderately productive waters. This work concerns an area in the northern Adriatic Sea defined by Berthon and Zibordi (2004) as a frontal area between case 1 and case 2 conditions according to the Morel and Prieur (1977) optical water type classification.

Water quality was assessed by (1) defining a two-component bio-optical model parameterised with specific inherent optical properties for the study area, (2) correcting the HICO^{TM} at-sensor radiances for both atmospheric and adjacent effects and (3) adopting a bio-optical model inversion technique. The study used data collected by the Aerosol Robotic Network-Ocean Colour (AERONET-OC) (Holben *et al.* 1998) at the Acqua Alta Oceanographic Tower (AAOT). These data were used both to run the atmospheric correction code and to validate HICO^{TM}-derived reflectance. Water-quality parameters (e.g. concentrations of chl-*a*, suspended particulate matter (SPM) and coloured dissolved organic matter (CDOM)) and water reflectances collected during the satellite overpass were also considered for validation purposes.

2. Materials and methods

2.1 *Study area and* in situ *measurements*

The northern Adriatic Sea is in the northernmost part of the Mediterranean and is characterized by a shallow depth (averaging 35 m). It receives approximately 20% of the total Mediterranean river run-off, mainly from the Po (the longest river in Italy), and its hydrodynamics are seasonally influenced by meteorological physical forcing (winds and tides). The northern Adriatic is also considered to be one of the most productive regions of the generally oligotrophic Mediterranean Sea. The largest phytoplankton blooms occur in its surface layers in late winter and in summer, they occur in the western part of the region. According to Hooker *et al.* (2004), the area alternates between case 1 and case 2 water types. Case 2 conditions are mainly due to the effects of local winds, which resuspend bottom sediments, and due to the discharge from the Po River and other rivers to the north (Adige, Piave, Tagliamento and Isonzo), which are sources of terrestrial particulate and dissolved matter. The Venice Lagoon and the Grado–Marano Lagoon lie along the northern Adriatic coastline, and the water exchange between the lagoons and the sea is governed by tide and contributes to the input of organic matter in the coastal waters (Ferrarin *et al.* 2013).

A 7-day cruise was undertaken in the study area (figure 1) in the second week of May 2012 to gather data for the purpose of calibrating a bio-optical model and assessing the HICO^{TM}-derived products, including water reflectance and water-quality parameters. At 18 stations (figure 1), discrete water samples were collected to measure absorption and concentration at two different depths (at the surface, by sampling the first integrated meter, and at the Secchi disk depth); then, the samples were filtered immediately *in situ* and were stored for subsequent laboratory analysis. The concentration

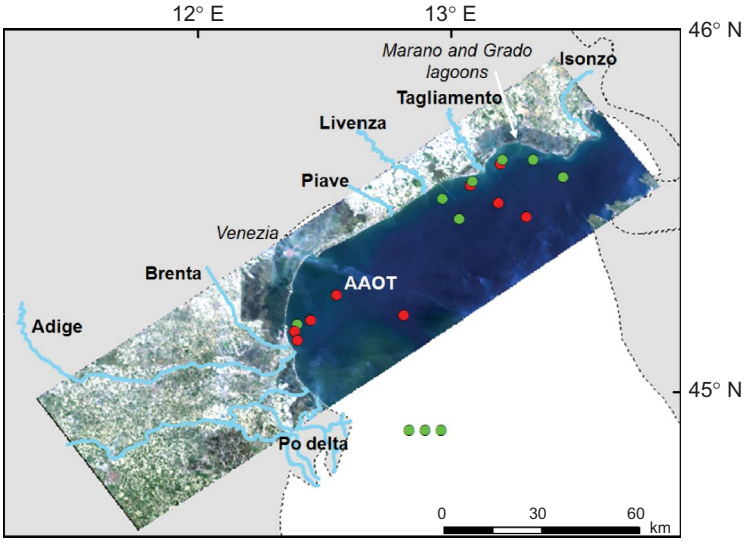

Figure 1. Study area with location of fieldwork activities carried out in the second week of May 2012 (green and red dots) and portion of Adriatic Sea imaged by HICO^{TM}. The stations visited on 10, 11 and 12 May 2012 are indicated with red dots; the data from these stations (which include also AERONET-OC AAOT site) allow us to validate the proposed methodology.

of chl-*a* was measured using the trichromatic method (APHA 1981), the concentration of SPM was measured with the gravimetric method (Van der Linde 1998) and the concentration of CDOM was assumed from the $a_{CDOM}(\lambda)$ at 440 nm (λ indicates the wavelength). The absorption spectra of particles retained on the filters, $a_p(\lambda)$, were obtained using the filter pad technique (Strömbeck and Pierson 2001) and were calculated according to Babin *et al.* (2003). The spectrophotometric determination and processing of the CDOM absorption spectra, $a_{CDOM}(\lambda)$, were derived from Kirk (1994). At the same stations where the water was sampled, remote-sensing reflectance (R_{rs}) values (omitting the wavelength dependence for the sake of clarity, apart from a few cases) were measured with a WISP-3 spectroradiometer (Water Insight, Wageningen, The Netherlands; Hommersom *et al.* 2012) in the optical range of 380–800 nm. A HydroScat-6 backscattering sensor (HOBILabs, Tucson, AZ, USA) was also used to estimate the backscattering coefficient of the particles ($b_{b\_p}(\lambda)$) (Maffione and Dana 1997).

Some of the *in situ* data used in this study were provided by the AERONET-OC AAOT station (Zibordi *et al.* 2009), located in the northern Adriatic approximately 15 km south-east of the Venice lagoon (12.51° E, 45.31° N); these data enabled us to identify the atmospheric parameters useful for the atmospheric correction of the HICO^{TM} image, as well as providing reference water reflectance spectra to validate the HICO^{TM}-derived reflectances.

2.2 *Bio-optical modelling*

The bio-optical model used in this study was based on works by Lee *et al.* (1998, 1999), where the $R_{rs}(\lambda)$ above water was a function of the subsurface radiance reflectance subsequently calculated as a function of the absorption $a(\lambda)$ and backscattering $b_b(\lambda)$

coefficients. To express the dependence of $a(\lambda)$ and $b_b(\lambda)$ on constituent concentrations (chl-*a*, CDOM and SPM), the spectral absorption coefficient, $a(\lambda)$, was modelled as

$$a(\lambda) = a_w(\lambda) + a_{CDOM}(440) \times e^{-S_{CDOM} \times (\lambda - 440)} + [\text{chl}{-}a] \times a^*_p(\lambda) \quad (1)$$

where, $a_w(\lambda)$ is the pure-water absorption (Smith and Baker 1981, Pope and Fry 1997), S_{CDOM} is the slope factor commonly used in modelling the absorption spectra of CDOM, [chl-*a*] is the concentration of chl-*a* and $a^*_p(\lambda)$ is the specific absorption of the particles, including phytoplankton and detritus. In this study, S_{CDOM} was established from each CDOM absorption spectrum measured, and the average slope (0.018) was used as the model parameter. The specific absorption for all particles, $a^*_p(\lambda)$, was the average value of the chlorophyll-specific particle absorption coefficients. In both cases, the average values were used because the data sets showed a low range of variation, with a coefficient of variation below 5% for both the CDOM slope and the chlorophyll-specific particle absorption coefficient.

The spectral backscattering coefficient, $b_b(\lambda)$, was modelled as

$$b_b(\lambda) = b_{b\_w}(\lambda) + [\text{SPM}] \times b^*_{b\_p}(\lambda) \quad (2)$$

where the backscattering coefficient of pure water, $b_{b\_w}(\lambda)$, was taken from Dall'Olmo and Gitelson (2006), [SPM] is the SPM concentration and $b^*_{b\_p}(\lambda)$ is the particle-specific backscattering coefficient. The backscattering coefficient of the SPM was modelled as an inverse power function of wavelength.

The scalars enabling the total $a(\lambda)$ and $b_b(\lambda)$ to be correlated with the subsurface remote-sensing reflectance and $R_{rs}(\lambda)$ were ascertained by fitting the forward run of the bio-optical model to *in situ* measurements of $R_{rs}(\lambda)$ taken at the 18 stations. The bio-optical model needs to be inverted to retrieve in-water constituent concentrations. This was done with the BOMBER software (Giardino *et al.* 2012) that inverts the bio-optical model using optimization techniques, while simultaneously retrieving water-quality parameters from remotely-sensed image atmospherically corrected to $R_{rs}(\lambda)$ values.

2.3 *Image processing*

A hyperspectral image was acquired by the HICO^{TM} sensor on 12 May 2012. The signal-to-noise ratio (SNR) of the at-the-sensor radiance in the HICO^{TM} data was investigated according to Gao (1993): for each sensor channel, the local standard deviation (LSD) was calculated for each block of pixels in the scene, identified using a moving window technique; the maximum value on the LSD histogram (representing the mean noise of the image) was then used to calculate the SNR, defined as the ratio between the mean value signal and the mean noise of the image.

The at-the-sensor radiance was converted into R_{rs} values above the water surface by adapting the algorithm presented in Bassani *et al.* (2010) to the HICO^{TM} image. The algorithm, called the HICO@CRI (HICO^{TM} atmospherically corrected reflectance image), is based on the atmospheric correction method presented in Vermote *et al.* (1997), using the 6SV radiative transfer code (Vermote *et al.* 1997, Kotchenova *et al.* 2008). The HICO@CRI also implements a correction for the adjacency effect according to Vermote *et al.* (1997) using the empirical formula

$$\rho_i = \rho_i^{\mathrm{s}} + \frac{t_{\mathrm{d}(\mu_{\mathrm{v}})_i}}{\mathrm{e}^{-\tau/\mu_{\mathrm{v}}}}[\rho_i^{\mathrm{s}} - < \rho_i^{\mathrm{s}} >] \tag{3}$$

where ρ_i is the at-ground reflectance of the ith channel, ρ_i^{s} is the reflectance with the environmental contribution and $\mathrm{e}^{-\tau/\mu_{\mathrm{v}}}$ and $t_{\mathrm{d}}(\mu_{\mathrm{v}})_i$ are the direct and diffuse components of the atmospheric transmittance along the target-sensor direction, respectively. These radiative quantities depend on the cosine of the viewing zenith angle, $\mu_{\mathrm{v}} = \cos\theta_{\mathrm{v}}$. The direct component is also defined by the total optical thickness, τ. The $< \rho_i^{\mathrm{s}} >$ is the average of the ρ_i^{s} for the ith channel, calculated on the whole image to ensure that the adjacency effect is removed from each pixel in the image.

The HICO@CRI inputs on aerosol optical thickness at 550 nm and precipitable water vapour were obtained at the AERONET-OC AAOT station, as retrieved from the direct sun algorithm at level 2.0 (Eck *et al.* 1999). The size distribution of the aerosol was obtained from the diffuse component corresponding to cloud-screened level 1.5 (Smirnov *et al.* 2000). The aerosol optical thickness at 550 nm (equal to 0.25) showed a low aerosol loading at the time of the HICO™ image acquisition, while the size distribution indicated an aerosol model dominated by fine particles, typical situation of the Adriatic Sea, as reported in Mélin *et al*. (2006).

3. Results and discussion

The SNR for the HICO™ data showed an average value of about 80 for all the 87 sensor channels for an *albedo* value of about 1%. In particular, the analysis showed a decreasing SNR for increasing wavelengths, with an average value of about 100 in the first 30 bands from 400 to 570 nm, the minimum value of 40 only being reached at bands 74 and 75, at around 825 nm. These results are consistent with the findings of Moses *et al.* (2012).

The methods used to assess water quality from the HICO™ image were assessed using *in situ* data collected at the 9 stations (of the 18) visited synchronously with the HICO™ overpass on 12 May 2012 (figure 1, red dots) and 2 days previously, since a 2-day mismatch between *in situ* data and acquired image is acceptable for the purpose of validating water-quality products based on the assumption that environmental variables (e.g. wind and river discharge) are fairly stable (Odermatt *et al.* 2010).

Figure 2 shows the convergence of the R_{rs} values obtained from atmospherically corrected image data, *in situ* spectroradiometric data and forward bio-optical modelling. The plot is given for the wavelengths measured by the radiometer at the AERONET-OC AAOT station (412, 442, 490, 530, 551, 667 and 868 nm), which are common to the HICO™ data and WISP-3 spectroradiometer (except for the band at 868 nm). The plotted spectra are the average values of the 9 measurements obtained at the stations measured in the footprint of the HICO™ during the satellite's overpass and on the 2 days beforehand. The HICO™-derived R_{rs} values were extracted from 3×3 pixel areas centred on the position of the *in situ* measurements, as suggested by Patt (2002) and Bailey and Werdell (2006). The *in situ* R_{rs} are the average values of WISP-3 measurements combined with the data gathered at the AERONET-OC AAOT station. The modelled R_{rs} values were obtained from the forward run of the bio-optical model using *in situ* data for the chl-*a*, SPM and CDOM concentrations.

Overall, a good consistency was obtained across the spectrum, with a relative root mean square error (RMSE) of 8% and 18%, respectively, when the modelled and HICO™ data were compared with *in situ* measurements. The HICO™-derived R_{rs}

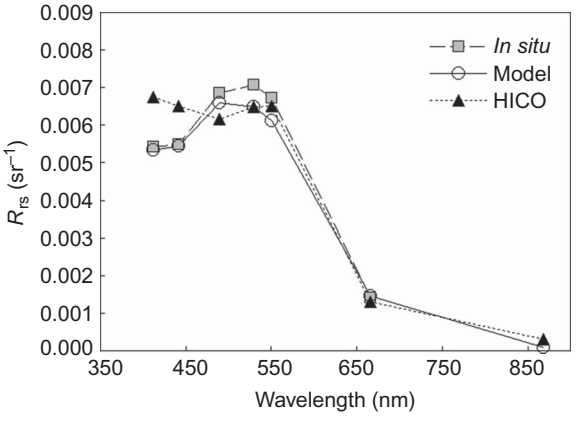

Figure 2. *In situ*, forward-modelled and HICO^{TM}-derived R_{rs} spectra. '*In situ*' spectrum is the average value measured with a WISP-3 spectroradiometer of the stations visited on 10-11-12 May 2012 plus the AERONET-OC AAOT site data (cf. figure 1, red dots).

values diverged at the shorter wavelengths (412 and 442 nm), however, showing an inverse trend between 412 and 490 nm. This mismatching behaviour might make estimations of CDOM from image data unpredictable. In fact, the R_{rs} values in the blue region are often used to retrieve CDOM concentrations because they are sensitive to changes in CDOM concentrations (Kutser *et al.* 2005). As in previous works (e.g. Giardino *et al.* 2007), the bio-optical model for mapping water quality was inverted by keeping a fixed CDOM concentration; the average value of 0.06 m^{-1} obtained from *in situ* measurements was used in the inversion performed with BOMBER.

Figure 3 presents the two BOMBER-retrieved HICO^{TM} maps with ranges of variation of 0–3 mg m^{-3} for chl-*a* and 0–4 g m^{-3} for SPM. The chl-*a* map shows quite low concentrations, with homogenous patterns except in the south-west, where there was a residual phytoplankton bloom induced by the nutrients discharged by the River Po and then dispersed by coastal currents. The SPM map likewise depicts fairly

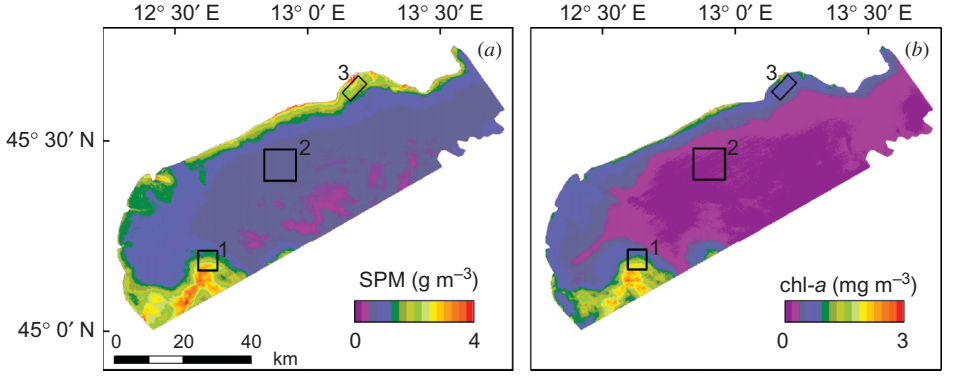

Figure 3. The BOMBER-retrieved products ((*a*) the SPM and (*b*) the chl-*a* concentrations) obtained from HICO^{TM} data acquired on 12 May 2013. The boxes indicate the areas where there were marked differences in the SPM and chl-*a* concentrations (these areas were also used to label the spectra in figure 4).

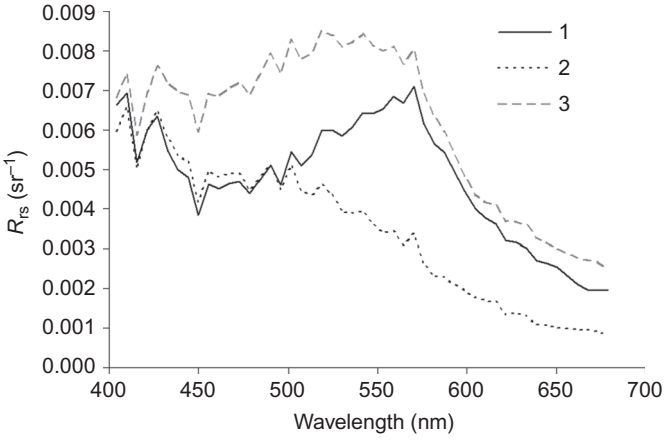

Figure 4. HICO^{TM}-derived R_{rs} spectra in waters affected by rivers plumes (1 and 3) and a clearer area (2), where were marked differences in the SPM and chl-*a* concentrations were found (cf. figure 3).

homogenous patterns with SPM concentrations around 1 g m^{-3}. The patchiest areas are in the coastal zones, particularly near the Grado and Marano lagoon, where the northern tributaries (figure 1) carry significant amounts of inorganic detritus. There is little correlation between the maps, save in the south-west, where the correspondence between SPM and chl-*a* is due to the load of nutrients discharged into the Adriatic Sea by the Po river causing a rapid increase in phytoplankton bloom, so that most of the suspended matter in this area is due to phytoplankton (Giani *et al.* 2001).

Figure 4 shows the HICO^{TM}-derived R_{rs} spectra coinciding with three areas where there were marked differences in the SPM and chl-*a* concentrations. These areas include waters affected by rivers plumes (figure 3, boxes 1 and 3) and a clearer area (figure 3, box 2) further away from the coast. The degree of variation in the three HICO^{TM}-derived spectra explains the chl-*a* and SPM patterns shown in figure 3. The highest spectra (#3 in figure 4) reveal the contribution of SPM due to discharge from northern tributaries; the spectra decreasing with wavelengths (#2 in figure 4) are typical of clear marine waters (Morel and Prieur 1977) and explain the low concentrations of both SPM and chl-*a* (figure 3, box 1) and the third spectra (#1 in figure 4) peaking at 570 nm explain the patterns of moderately high chl-*a* concentrations found around the mouth of the Po river. Finally, all the spectra show a trend with peaks and dips at shorter wavelengths, where the HICO^{TM} data appear to be less reliable (figure 4).

Figure 5 shows two scatter plots depicting the HICO^{TM}-derived estimations of the chl-*a* and SPM concentrations versus the *in situ* measurements obtained at the 9 stations sampled at the time of the HICO^{TM} overpass (figure 1, red dots). The HICO^{TM} image was again averaged on a 3 × 3 pixel area centred on the location of the sampling stations. The HICO^{TM}-derived SPM concentration was consistent with the *in situ* data, with a correlation coefficient r of 0.92, a coefficient of determination R^2 of 0.85 and a relative RMSE of 25.1%, and coming close to the 1:1 line with a slope of 0.985 (figure 5(*a*)). The chl-*a* data validation was positive too, showing an r of 0.84, an R^2 of 0.71, a relative RMSE of 16.5% and a slope of 1.013 (figure 5(*b*)).

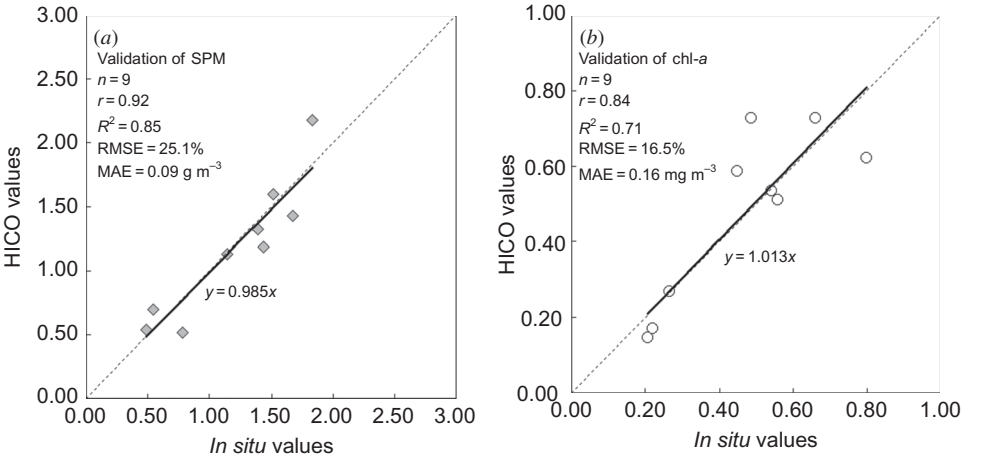

Figure 5. Scatter plots of HICO^{TM}-derived products and *in situ* concentrations measured in 9 stations (cf. figure 1 red dots): (*a*) the SPM plot and (*b*) the chl-*a* plot. The statistics of fitting are given as correlation coefficient (r), coefficient of determination (R^2), relative root means square error (RMSE) and mean absolute error (MAE). In both plots, the number of samples (n) is 9 and the 1:1 line is plotted as dotted lines.

4. Conclusions

A HICO^{TM} image of the northern Adriatic Sea was acquired on 12 May 2012 and was used for assessing water-quality parameters. Physically-based methods were used to convert the at-the-sensor radiance into R_{rs} values (HICO@CRI, Bassani *et al.* 2010) and to retrieve synchronous water-quality parameters from image data (BOMBER, Giardino *et al.* 2012). These methods were parameterised using *in situ* measurements to characterize both the optical properties of atmosphere and the specific inherent optical properties of water.

The performance of the proposed method was measured by comparing the R_{rs} values obtained by forward modelling, *in situ* measurements and atmospherically corrected HICO^{TM} data (including a correction for adjacent effects). The match of the R_{rs} spectra was sufficient for the purpose of this study, but further investigations are needed at the shortest wavelengths to obtain a better consistency of the HICO^{TM} data.

This study confirms that the HICO^{TM} has a good enough SNR and spatial resolution for assessing the complexity of coastal features, enabling local phenomena to be distinguished. While we await the next generation of space-borne hyperspectral imagers (e.g. SENTINELs, HYSPIRY, PRISMA, EnMap), the HICO^{TM} facility has given us an opportunity to simulate and verify the new sensors' capabilities.

Acknowledgements

This work was undertaken as part of the CLAM-PHYM Project, funded by the Italian Space Agency (ASI, contract No. I/015/11/0); co-funding was provided by the projects CYAN-IS-WAS (a scientific and technological cooperation between Italy and the Kingdom of Sweden) and RITMARE (MIUR-CNR). We are grateful to G. Zibordi for providing data of the AERONET-OC AAOT site. *In situ* data were collected thanks to the 'ENV-ADRI-LTER-3 & CLAM-PHYM-Nord' oceanographic cruise. We are very grateful to all those who took part in the cruise and to the staff

on board the CNR's URANIA vessel. The HICO™ image used for this study was provided by the Naval Research Laboratory, USA, and the Oregon State University. We are grateful to the anonymous reviewers for helpful comments on the manuscript.

References

APHA, 1981, *Standard Methods for the Examination of Water and Wastewater*, 14th ed. (Washington, DC: APHA).

Babin, M., Stramski, D., Ferrari, G.M., Claustre, H., Bricaud, A., Obolensky, G. and Hoepffner, N., 2003, Variations in the light absorption coefficients of phytoplankton, nonalgal particles, and dissolved organic matter in coastal waters around Europe. *Journal of Geophysical Research*, **108**, 3211 pp.

Bailey, W.S. and Werdell, J.P., 2006, A multi-sensor approach for the on-orbit validation of ocean color satellite data products. *Remote Sensing of Environment*, **102**, pp. 12–23.

Bassani, C., Cavalli, R.M. and Pignatti, S., 2010, Aerosol optical retrieval and surface reflectance from airborne remote sensing data over land. *Sensors*, **10**, pp. 6421–6438.

Berthon, J.F. and Zibordi, G., 2004, Bio-optical relationships for the northern Adriatic Sea. *International Journal of Remote Sensing*, **25**, pp. 1527–1532.

Dall'olmo, G. and Gitelson, A.A., 2006, Effect of bio-optical parameter variability and uncertainties in reflectance measurements on the remote estimation of chlorophyll-a concentration in turbid productive waters: modeling results. *Applied Optics*, **45**, pp. 3577–3592.

Eck, T.F., Holben, B.N., Reid, J.S., Dubovik, O., Smirnov, A., O'neill, N.T., Slutsker, I. and Kinne, S., 1999, Wavelength dependence of the optical depth of biomass burning, urban, and desert dust aerosols. *Journal of Geophysical Research: Atmospheres*, **104**, pp. 31333–31349.

Ferrarin, C., Ghezzo, M., Umgiesser, G., Tagliapietra, D., Camatti, E., Zaggia, L. and Sarretta, A., 2013, Assessing hydrological effects of human interventions on coastal systems: numerical applications to the Venice Lagoon. *Hydrology and Earth System Sciences*, **17**, pp. 1733–1748.

Gao, B., 1993, An operational method for estimating signal-to-noise ratios from data acquired with imaging spectrometers. *Remote Sensing of Environment*, **43**, pp. 23–33.

Giani, M., Boldrin, A., Matteucci, G., Frascari, F., Gismondi, M. and Rabitti, S., 2001, Downward fluxes of particulate carbon, nitrogen and phosphorus in the north-western Adriatic Sea. *The Science of the Total Environment*, **266**, pp. 125–134.

Giardino, C., Brando, V.E., Dekker, A.G., Strömbeck, N. and Candiani, G., 2007, Assessment of water quality in Lake Garda (Italy) using Hyperion. *Remote Sensing of Environment*, **109**, pp. 183–195.

Giardino, C., Candiani, G., Bresciani, M., Lee, Z., Gagliano, S. and Pepe, M., 2012, BOMBER: a tool for estimating water quality and bottom properties from remote sensing images. *Computers & Geosciences*, **45**, pp. 313–318.

Gitelson, A.A., Gao, B.C., Li, R.R., Berdnikov, S. and Saprygin, V., 2011, Estimation of chlorophyll-a concentration in productive turbid waters using a Hyperspectral Imager for the Coastal Ocean – the Azov Sea case study. *Environmental Research Letters*, **6**, 6 pp.

Holben, B.N., Eck, T.F., Slutsker, I., Tanre, D., Buis, J.P., Setzer, A., Vermote, E., Reagan, J.A., Kaufman, Y.J., Nakajima, T., Lavenu, F., Jankowiak, I. and Smirnov, A., 1998, AERONET – a federated instrument network and data archive for aerosol characterization. *Remote Sensing of Environment*, **66**, pp. 1–16.

Hommersom, A., Kratzer, S., Laanen, M., Ansko, I., Ligi, M., Bresciani, M., Giardino, C., Beltrán-Abaunza, J.M., Moore, G., Wernand, M. and Peters, S., 2012, Intercomparison in the field between the new WISP-3 and other radiometers (TriOS Ramses, ASD FieldSpec, and TACCS). *Journal of Applied Remote Sensing*, **6**, pp. 63615–63615.

Hooker, S.B., Zibordi, G., Berthon, J.F. and Brown, J.W., 2004, Above-water radiometry in shallow coastal waters. *Applied Optics*, **43**, pp. 4254–4268.

Kirk, J.T.O., 1994, *Light & Photosynthesis in Aquatic Ecosystems*, 2nd ed., 509 pp (New York: Cambridge University Press).

Kotchenova, S.Y., Vermote, E.F., Levy, R. and Lyapustin, A., 2008, Radiative transfer codes for atmospheric correction and aerosol retrieval: intercomparison study. *Applied Optics*, **47**, pp. 2215–2226.

Kutser, T., Pierson, D.C., Kallio, K., Reinart, A. and Sobek, S., 2005, Mapping lake CDOM by satellite remote sensing. *Remote Sensing of Environment*, **94**, pp. 535–540.

Lee, Z., Carder, K.L., Mobley, C.D., Steward, R.G. and Patch, J.S., 1998, Hyperspectral remote sensing for shallow waters. I. A semianalytical model. *Applied Optics*, **37**, pp. 6329–6338.

Lee, Z., Carder, K.L., Mobley, C.D., Steward, R.G. and Patch, J.S., 1999, Hyperspectral remote sensing for shallow waters. 2. Deriving bottom depths and water properties by optimization. *Applied Optics*, **38**, pp. 3831–3843.

Lucke, R.L., Corson, M., McGlothlin, N.R., Butcher, S.D., Wood, D.L., Korwan, D.R., Li, R., Snyder, W.A., Davis, C.O. and Chen, D.T., 2011, Hyperspectral Imager for the Coastal Ocean: instrument description and first images. *Applied Optics*, **50**, pp. 1501–1516.

Maffione, R.A. and Dana, D.R., 1997, Instruments and methods for measuring the backward-scattering coefficient of ocean waters. *Applied Optics*, **36**, pp. 6057–6067.

Mélin, F., Clerici, M., Zibordi, G. and Bulgarelli, B., 2006, Aerosol variability in the Adriatic Sea from automated optical field measurements and Sea-viewing Wide Field-of-view Sensor (SeaWiFS). *Journal of Geophysical Research: Atmospheres*, **111**, D22201.

Morel, A. and Prieur, L., 1977, Analysis of variations in ocean color. *Limnology and Oceanography*, **22**, pp. 709–722.

Moses, W.J., Bowles, J.H., Lucke, R.L. and Corson, M.R., 2012, Impact of signal-to-noise ratio in a hyperspectral sensor on the accuracy of biophysical parameter estimation in case II waters. *Optics Express*, **20**, pp. 4309–4330.

Odermatt, D., Giardino, C. and Heege, T., 2010, Chlorophyll retrieval with MERIS Case-2-Regional in perialpine lakes. *Remote Sensing of Environment*, **114**, pp. 607–617.

Patt, F.S., 2002, Navigation algorithms for the SeaWiFS mission. In *SeaWiFS Postlaunch Technical Report Series*, S.B. Hooker and E.R. Firestone (Eds.) (Greenbelt, MD: NASA Goddard Space Flight Center).

Pope, R.M. and Fry, E.S., 1997, Absorption spectrum (380–700 nm) of pure water. II. Integrating cavity measurements. *Applied Optics*, **36**, pp. 8710–8723.

Smirnov, A., Holben, B.N., Eck, T.F., Dubovik, O. and Slutsker, I., 2000, Cloud-screening and quality control algorithms for the AERONET database. *Remote Sensing of Environment*, **73**, pp. 337–349.

Smith, R.C. and Baker, K.S., 1981, Optical properties of the clearest natural waters (200–800 nm). *Applied Optics*, **20**, pp. 177–184.

Strömbeck, N. and Pierson, E., 2001, The effects of variability in the inherent optical properties on estimations of chlorophyll a by remote sensing in Swedish freshwater. *The Science of the Total Environment*, **268**, pp. 123–137.

Tufillaro, N., Davis, C.O. and Jones, K.B., 2010, Indicators of plumes from HICO^{TM}. In *XX Ocean Optics,* 27 September–1 October 2011, Anchorage, AK.

Van der Linde, D., 1998, *Protocol for Total Suspended Matter* (Ispra: CEC-JRC) (Technical Note).

Vermote, E.F., Tanré, D., Deuze, J.L., Herman, M. and Morcette, J.J., 1997, Second simulation of the satellite signal in the solar spectrum, 6S: an overview. *IEEE Transactions on Geoscience and Remote Sensing*, **35**, pp. 675–686.

Zibordi, G., Holben, B., Slutsker, I., Giles, D., D'alimonte, D., Mélin, F., Berthon, J.-F., Vandemark, D., Feng, H., Schuster, G., Fabbri, B.E., Kaitala, S. and Seppälä, J., 2009, AERONET-OC: a network for the validation of ocean color primary products. *Journal of Atmospheric and Oceanic Technology*, **26**, pp. 1634–1651.